Centrum voor Wiskunde en Informatica

REPORT*RAPPORT*

Superfast fronts of impact ionization in initially unbiased layered semiconductor structures

P.B. Rodin, U.M. Ebert, W.H. Hundsdorfer, I.V. Grekhov

Superfast Fronts of Impact Ionization
in Initially Unbiased Layered Semiconductor Structures

P. Rodin[1,2], U. Ebert[2], W. Hundsdorfer[2], and I.V. Grekhov[1]

[1] *Ioffe Physicotechnical Institute, Politechnicheskaya 26, 194021, St. Petersburg, Russia,*
[2] *CWI, P.O.Box 94079, 1090 GB Amsterdam, The Netherlands*

ABSTRACT

We present results of numerical simulations of superfast impact ionization fronts in initially unbiased layered semiconductor structures. We demonstrate that when a sufficiently sharp voltage ramp $A > 10^{12}$ V/s is applied in the reverse direction to an initially unbiased Si $p^+ - n - n^+$-structure connected in series with a load R, then after some delay the system will reach the high conductivity state via the propagation of a superfast impact ionization front which leaves a dense electron-hole plasma behind. The front travels towards the anode with a velocity v_f several times larger than the saturated drift velocity of electrons v_s. The excitation of the superfast front corresponds to the transition from the common avalanche breakdown of a semiconductor structure to a collective mode of streamer-like breakdown.

For a structure with typical thickness of $W \sim 100$ μm, first there is a delay of about 1 ns during which the voltage reaches a value of several kilovolts. Then, as the front is triggered, the voltage abruptly breaks down to several hundreds of volts within ~ 100 ps. This provides a voltage ramp of up to $\sim 2 \cdot 10^{13}$ V/s, hence up to 10 times sharper than the externally applied ramp. We unravel the source of initial carriers which trigger the front and explain the origin of the time delay in triggering the front. Further we identify the mechanism of front propagation and discuss the possibility to excite superfast ionization fronts not in layered structures but in bulk semiconductors.

I. INTRODUCTION

Traveling front patterns are common nonlinear phenomena in various spatially extended systems far from equilibrium[1–3]. In gases and solids exposed to a strong external electrical field, a conducting region might penetrate an essentially nonconducting region in the form of a field driven impact ionization front. The front is characterized by a space charge that screens the electric field from the highly ionized plasma region. Depending on the initial degree of ionization, the polarity of the applied voltage and on the importance of nonlocal ionization reactions, the ionization process takes place inside or in the vicinity of the screening front[4–17]. The structure of the impact ionization front transverse to the direction of front propagation depends on the experimental setup, e.g., on the form of the electrodes and other outer boundaries, the voltage, *etc.*: In long narrow glass tubes filled with gas, planar ionization fronts have been observed[6], whereas in many other discharges in gases or solids the ionization front propagates at the tip of a long and narrow highly conducting channel, the so-called streamer[4–16], and the propagation process is essentially three-dimensional. Ionization fronts of various shapes — plane fronts, finger-shaped streamers, concentrical fronts in samples with Corbino geometry *etc.* — have been observed in semiconductors, including bulk semiconductors[7], semiconductor films of different contact geometries[3] and layered structures of semiconductor devices[18–20].

In this article we deal with *superfast impact ionization fronts* in layered semiconductor structures which propagate many times faster than the saturated drift velocity of free carriers v_s and create a dense electrically screened electron-hole plasma. The superfast front velocity indicates that the front propagation represents a collective phenomenon which makes this mode of impact ionization breakdown important from a fundamental point of view and also provides the basis of numerous applications. This spectacular mode of the impact ionization breakdown of layered $p^+ - n - n^+ -$ structures has been discovered several decades ago[21–25] and is often coined as TRAPATT-mode[22] (for "TRApped Plasma Avalanche Triggered Transit"). It underlies the operation of devices such as TRAPATT-diodes[22] used as microwave generators (output pulse power 10^3 W) and silicon avalanche sharpening diodes (SAS) used in pulse power electronics (output pulse power 10^7 W)[23–28]. A TRAPATT-diode is operated in a regime of periodic oscillations where the impact ionization fronts almost immediately follow each other, so that the nonequilibrium carriers from the previous front passage play an essential role in the excitation of the next front. In contrast, for pulse sharpening diodes the time interval between two subsequent front passages is large compared to the system relaxation time and each excitation of a front represents an independent event. Here we concentrate entirely on the last situation.

Superfast impact ionization fronts are known to occur in $p^+ - n - n^+ -$structures that initially are subject to a reverse bias V_0 which is closely below the voltage of stationary avalanche breakdown U_a [23,25–28]. If the applied reverse voltage is being further increased like $V(t) = V_0 + A\,t$ with a sufficiently high rate A, the impact ionization starts near the $p^+ -$layer, where the electrical field takes its maximal value, and develops into an impact ionization front which travels towards the $n^+ -$layer with a velocity $v_f > v_s$. It leaves a dense electron hole plasma behind with an electron concentration N much higher than the doping level in the $n-$base N_d.

The main purpose of this article is to demonstrate that the initial bias V_0 is in fact *not needed*, and switching due to the propagation of a superfast front can be succesfully achieved in *initially unbiased structures* for $V_0 = 0$. We present numerical simulations of this mode of impact ionization breakdown. We unravel the source of mobile carriers that initialize the impact ionization and that provide the background ionization needed for propagation with velocity $v_f > v_s$. We argue that the excitaton of the superfast front generally corresponds to the transition from the common avalanche breakdown of a semiconductor structure to a collective mode of *streamer*-like breakdown and relate the impact ionization fronts in layered semiconductor structures to theoretical studies of streamer propagation in gases and solids[10–16].

The paper is organized as follows. After introducing the semiconductor structure and the physical model in Sec. II, in Sec. III we present results of numerical simulations for one typical set of parameters and describe the main stages of the superfast switching process. Here we also discuss the applicability of the continuum approximation to our problem. Sec. IV deals with the question how the switching process depends on the structure length and the voltage ramp applied to the device. In Sec. V, we discuss the mechanism of front propagation and the avalanche-to-streamer transition occuring at the moment when the front is triggered. In Sec. VI, we compare ionization fronts in initially unbiased and biased structures and survey alternative sources of initial carriers which can trigger the front. Sec. VII briefly summarizes our results.

II. THE MODEL

The excitation of impact ionization fronts has been observed in experiments in the large family of Si[23,24,29,30] or GaAs[31–33] layered semiconductor structures. Here we shall concentrate on the basic case of a Si diode $p^+ - n - n^+ -$structure with sharp $p^+ - n$ and $n - n^+ -$transitions. Typical parameters are the following: the width of the $n-$base W is 100 to 300 μm, the area S of the cross-section transverse to the direction of current is approximately 0.005 to 0.05 cm^2, the doping levels are $N_d \approx 10^{14}$ cm^{-3} in the $n-$base, and $N_{a,d}^+ \approx 10^{19} - 10^{20}$ cm^{-3}

in the contact p^+- and n^+-layers, respectively. The device is connected to the voltage source $V(t)$ in series with the load resistance $R \sim 50 - 100 \ \Omega$ as sketched in Fig. 1 and operated at room temperature. Note that we have chosen to put the n^+-contact on the left hand side at $z = 0$ in all figures and equations throughout the paper. This choice allows us to work with positive electrical fields for reverse bias.

The dynamics of charge carriers is described in the drift-diffusion approximation by the following standard set of continuity and transport equations

$$\frac{\partial n}{\partial t} - \nabla \cdot \frac{\mathbf{J}_n}{q} = G(n, p, |E|), \tag{1}$$

$$\frac{\mathbf{J}_n}{q} = v_n(|E|) \ \hat{\mathbf{e}} \ n + D_n \ \nabla n,$$

$$\frac{\partial p}{\partial t} + \nabla \cdot \frac{\mathbf{J}_p}{q} = G(n, p, |E|), \tag{2}$$

$$\frac{\mathbf{J}_p}{q} = v_p(|E|) \ \hat{\mathbf{e}} \ p - D_p \ \nabla p,$$

together with the Poisson equation for the electric field

$$\nabla \cdot \mathbf{E} = \frac{q}{\varepsilon \varepsilon_0} \left(p - n + N_d(z) - N_a(z) \right), \tag{3}$$

$$\mathbf{E} = -\nabla \Phi, \qquad \hat{\mathbf{e}} = \frac{\mathbf{E}}{|\mathbf{E}|}.$$

Here n and p are concentrations of electrons and holes, respectively. Φ and $\mathbf{E}$ are electrical potential and field, $q > 0$ is the elementary charge, and $\mathbf{J}_{n,p}$ are the current densities carried by electrons and holes, respectively. ε and ε_0 are the permittivity of the material and the absolute permittivity. $D_{n,p}$ are the diffusion coefficients of electrons and holes. $N_d(z)$ and $N_a(z)$ are the concentration of donors and acceptors, respectively, which form the doping profile of the $p^+ - n - n^+-$structure along the $z-$direction.

We here assume that all processes are uniform in the directions orthogonal to the cathode-anode direction z. We hence neglect transverse instablities of a planar front[34−38] and consider the problem in a one-dimensional approximation. Next, given the fact that physical processes relevant for the propagation of the ionization front develop in the bulk of the $n-$base, we restrict our consideration to the $n-$base area $0 < z < W$. We impose mixed boundary conditions for concentrations $\partial_z n = 0$, $p = 0$ at $z = 0$ and $\partial_z p = 0$, $n = 0$ at $z = W$, that reflect the different effect of the contact p^+- and n^+-layers on electron and hole concentrations in the $n-$base. Since $N^+_{a,d} \gg N_d$ the voltage drop at the contact layers is also negligible.

We set the potential $\Phi(W, t) \equiv 0$ for all times t and denote the voltage applied to the device with $U(t) \equiv \Phi(0, t) > 0$. It is related to the voltage $V(t) > 0$ of the power source by Kirchhoff's equation

$$V(t) = U(t) + RS \ J(t), \tag{4}$$

$$J(t) \equiv J_n(z, t) + J_p(z, t) + \varepsilon \varepsilon_0 \frac{\partial E(z, t)}{\partial t}, \tag{5}$$

where $J(t)$ is the total (conductive and displacement) current density in the system which is conserved in space $\partial_z J = 0$ in one-dimensional systems, S is the area of the cross-section and $E \equiv E_z$. Averaging (5) over the system length, we represent (4) as[39,3]

$$RC \frac{dU}{dt} = V(t) - U - \frac{RS}{W} \int_0^W \left(J_n(z, t) + J_p(z, t) \right) dz, \tag{6}$$

$$C = \frac{\varepsilon \varepsilon_0 S}{W},$$

where C is the intrinsic capacitance of the semiconductor structure.

The applied voltage $V(t)$ typically represents a sinusoidal pulse $V(t) = V_0 + V_1 \sin(2\pi t/T)$, or a combination of such a pulse for $t < T/4$ with a plateau $V = V_0 + V_1$ for $t > T/4$. Since the duration of the fast impact ionization breakdown is usually smaller than $T/4$, in most cases the applied voltage can be approximated by the linear function

$$V(t) = V_0 + A \ t, \qquad A \equiv 2\pi V_1/T, \tag{7}$$

where A is the voltage ramp.

For the dependencies of electron and hole velocities v_s and v_p on the electrical field E in Si, we use the simplified version of the approximation suggested in Ref. 40

$$v_n(|E|) = v_s \ \frac{|E|}{E_{sn} + |E|}, \qquad v_p(|E|) = v_s \ \frac{|E|}{E_{sp} + |E|}, \tag{8}$$

$$\text{where} \qquad v_s = 10^7 \ \text{cm/s}, \tag{9}$$

$$E_{sn} = 8.0 \cdot 10^3 \ \text{V/cm}, \qquad E_{sp} = 2.32 \cdot 10^4 \text{V/cm}.$$

These approximations describe the monotonic transition from the low-field Ohmic regime $v_{n,p}(E) = \mu_{n,p} E$ (low-field mobilities are given by $\mu_{n,p} = v_s/E_{sn,sp}$) to the high-field transport with saturated drift velocity v_s due to the scattering of carriers on optical phonons. Diffusion coefficients are determined by the Einstein relation $D_{n,p}/\mu_{n,p} = kT/q$, where T is the temperature and k is Boltzmann's constant.

The term $G(n, p, |E|)$ describes the generation of charge carriers due to impact ionization both by electrons and holes. It is chosen as

$$G(n, p, |E|) = \alpha_n(|E|) \ v_n(|E|) \ n \ \Theta(n - n_{cut}) \tag{10}$$
$$+ \ \alpha_p(|E|) \ v_p(|E|) \ p \ \Theta(p - p_{cut}),$$

$$\alpha_n(|E|) \equiv \alpha_{ns} \ e^{-b_n/|E|}, \ \alpha_n(|E|) \equiv \alpha_{ps} \ e^{-b_p/|E|}, \tag{11}$$

where $\Theta(x)$ is the step-function, and the impact ionization coefficients and the characteristic fields are given by[41]

$$\alpha_{ns} = 7.4 \cdot 10^5 \ \text{cm}^{-1}, \ \alpha_{ps} = 7.25 \cdot 10^5 \ \text{cm}^{-1},$$
$$b_n = 1.1 \cdot 10^6 \ \text{V/cm}, \ b_p = 2.2 \cdot 10^6 \ \text{V/cm}. \tag{12}$$

3

The cut-offs n_{cut} and p_{cut} have been introduced in (10) to exclude unphysical effects which otherwise appear for concentrations below the limits of the continuum approximation. The necessity and validity of these cut-offs will be discussed in Sec. III.E.

The electrical fields relevant to the propagation of impact ionization fronts correspond to the interval $2 \cdot 10^5 - 4 \cdot 10^5$ V/cm, In this interval the impact ionization coefficients (11) rapidly increase with electrical field. The field $E_a \approx 2 \cdot 10^5$ V/cm can be considered as an effective threshold of the impact ionization. Since $E_s \ll E_a$, the drift velocities are saturated in the impact ionization region.

On nanosecond time scale recombination can be neglected. Though the diffusion term is taken into account in the transport equations (1), (2), the diffusion turns out to be negligible compared to the drift and has no impact on our results.

For the numerical simulation a uniform space-time grid has been selected. The spatial discretization is based on a conservative formulation, in terms of fluxes describing the inflow and outflow over cells $[x - \Delta x/2, x + \Delta x/2]$, where Δx is the grid width in space. The number of grid points used in these simulations was of the order of several thousands both in time and space, to obtain sufficiently accurate numerical results. The diffusive fluxes have been approximated in a standard fashion[42] with second order accuracy. For the convective fluxes a third order upwind biased formula has been chosen in order to reduce the numerical oscillations that are common with second order central fluxes. Time discretization is based on a second order backward differentiation formula. The temporal backward differentiation formula gives an implicit system that is solved at each time step. For reasons of accuracy the time step Δt is chosen small compared to $\Delta x/v_s$, where v_s is the upper bound of the drift (convective) velocity, and with such small step size the implicit system can be solved by a straightforward functional iteration. Details on these spatial and temporal discretizations can be found in Ref. 43.

III. NUMERICAL SOLUTIONS - THE BASIC EXAMPLE

In this section we present numerical solutions of our model for a typical set of parameters: the width of the n-base is taken to be $W = 150\ \mu$m, its doping levels are $N_d = 10^{14}$ cm^{-3} and $N_a = 0$, and its transverse area is $S = 0.02$ cm^2. The resistance of the load is $R = 50\ \Omega$. The voltage ramp is $A = 2$ kV/ns, the initial voltage $V_0 = 0$. The cut-off at low concentrations is taken as $n_{cut} = p_{cut} = 10^9$ cm^{-3}.

The basic features of the numerical solution for these parameters are summarized in Fig. 2 which shows the voltage at the device $U(t)$ and the total current through the device $I(t) = S\ J(t)$. Up to the time $t \approx 1.5$ ns, the

voltage $U(t)$ follows the increase of the applied voltage $V(t)$ and reaches the value $U \approx 3$ kV which exceeds the voltage of stationary breakdown[18] $U_a \approx 1.7$ kV nearly twice. Within the next approximately 230 ps, it drops to the residual voltage $U_a \approx 450$ V, so that suddenly almost the complete $V(t)$ is applied to the external load R. The abrupt decay of $U(t)$ after $t \approx 1.5$ ns shows a "fine structure" at $t \approx 1.6$ ns, reflecting a change in the internal breakdown dynamics. The average voltage drop $|dU/dt| \approx 10$ kV/ns during the switching indicates a substantial sharpening of the externally applied pulse $V(t)$.

In the following subsections we discuss the different stages of the internal dynamics which underlie this switching process. The corresponding spatial profiles at different time steps are shown in Fig. 3.

A. The latent stage (Fig. 3(a), $0 < t < 1.47$ ns)

Initially the $n-$base is neutral since the major carriers (electrons) compensate the space charge of the donors: $n \approx N_d = 10^{14}$cm^{-3}. At room temperature, the concentration $p \approx N_T \approx 10^{5 \ldots 6}$cm^{-3} of the minor carriers (holes) is much lower than N_d and can be neglected. As the voltage applied to the device increases, the homogeneously distributed electrons drift towards the n^+-contact where they are being extracted from the $n-$base. The moving electron package leaves naked donors behind. Consequently, the device splits into *depleted region*, which is free of major carriers, and *neutral region*, where the major carriers are still present. The slope of the electrical field in the depleted region is determined by the space charge of naked donors: $dE/dz = qN_d/\varepsilon\varepsilon_0$. The electric field $E_0(t)$ in the *neutral region* is constant in space: $dE_0/dz = 0$. In the following, we will refer to the boundary between these two regions as to the *extraction front*. The velocity of the extraction front is the electron drift velocity $v_n(E_0)$ corresponding to the electrical field E_0 in the neutral layer. It is bounded from above by the saturated drift velocity v_s.

Although the maximum value of the electrical field which is reached at the right boundary, already for $t > 1$ ns overcomes the effective threshold $E_a \approx 2 \cdot 10^5$ V/cm of impact ionization in Si, the ionization in the depleted region does not develop due to the absence of initial carriers. Rather, with increase of the applied voltage a moderate impact ionization by electrons starts in the neutral region: despite of the relatively low electrical field E_0, the ionization reaction does develop due to the high electron concentration $n \approx N_d$. Though the total amount of generated free carriers is much smaller than N_d, a substantial concentration of holes $p \sim 10^{12}$ cm^{-3} much bigger than the thermal ionization N_T is generated in the neutral region. The holes move to the right and eventually penetrate the region of high electric field near the p^+-contact.

B. Triggering of the impact ionization front
(Fig. 3(b), 1.47 ns < t < 1.60 ns)

As soon as drifting holes reach high electrical fields in the depleted region, the impact ionization by holes becomes efficient (curve 4 on Fig. 3(a) shows the beginning of the avalanche multiplication in the depleted region). The generated electrons and holes in the high field region then multiply further and eventually form the nucleus of an electron-hole plasma capable to screen the electrical field [cf. curve 2 in Fig. 3(b)]. Since the concentration of holes that initialize the impact ionization decreases towards the right, the multiplication process does not start exactly at the right boundary of the $n-$base where the electric field is maximal. But within approximately 50 ps, the generated electron–hole plasma completely screens the electric field inside the nucleus. The charge generation by impact ionization continues on the left side of the nucleus where the field remains high, providing the basis for further expansion of the conducting region into the depletion region in the form of a propagating *impact ionization front.*

The screening of the electric field, that is due to the collective dynamics of electron and holes, is the central feature of the breakdown mode under consideration here. It makes this mode essentially different from the conventional *avalanche* scenario of impact ionization breakdown[18], where electrons and holes drift apart during the ionization process. We discuss this transition in more detail in Sec. V.

At the moment when the impact ionization front is triggered, the extraction front has not necessarily reached the n^+-contact, and there can be a high concentration of electrons $n \approx N_d$ at the left side of the $n-$base. Therefore, in general, the impact ionization front and the extraction front can coexist in the system for some time.

C. Propagation of the impact ionization front
(Fig. 3(c), 1.60 ns < t < 1.66 ns)

The third stage corresponds to the propagation of the *impact ionization front* whose velocity v_f exceeds the saturated drift velocity v_s. For the parameters corresponding to Figs. 2,3 we obtain $v_f \approx 5v_s$. Hence the superfast front propagation is a collective process which is not directly based on the drift motion of the individual carriers. The velocity $v_f > v_s$ becomes possible due to the local multiplication of a small amount of mobile carriers that are present in the depleted region. These carriers are holes that are being generated in the neutral region on the left and drift to the high field region on the right. The inner structure of the superfast front and the mechanism of its propagation are discussed in more detail in Sec. V.

The current density and the maximum electrical field increase as the front propagates. Consequently, the plasma concentration behind the front also increases.

Since the front velocity is much higher than the saturated drift velocity, the concentration profiles in the plasma behind the front remain frozen. Due to the interaction with the external load the voltage at the device decreases with increase of the current.

As the front propagates, the electrical field at the right side of the system starts to increase again due to the separation of the generated electrons and holes near the $p^+ - n-$junction. Electrons move to the left and holes to right. This leads to the formation of a positively charged layer adjacent to the right boundary.

D. Collision of the impact ionization front and the extraction front (Fig. 3(d), 1.66 ns < t < 1.73 ns)

If all major carriers are removed from the system before the ionization front reaches the n^+-contact, it continues to propagate up to the moment when the whole $n-$base is filled with a dense electron-hole plasma. Otherwise the ionization front and the extraction front collide. After the collision the character of the process changes due to the presence of a high concentration of major carriers in the area with strong electrical field: the ionization front passage is essentially terminated and we observe a quasiuniform impact ionization in the neutral area. As the concentration increases, the electrical field on the left side of the structure decreases (Fig. 3(d), curves 1,2,3). For the chosen set of parameters this stage is not very well pronounced, since the extraction front is close to the n^+-layer at the moment of collision. However, the situation becomes different in longer structures as well as for an earlier start of the impact ionization front caused by a higher voltage ramp applied to the device. Regimes with and without collision are both possible depending on the $n-$base length W, the voltage ramp A and the initial bias V_0.

We should stress that generally the propagation of an ionization front generates a much higher concentration of free carriers than quasiuniform breakdown. Indeed, during the fast propagation of an impact ionization front, a region of high electric field passes through the device and hence the ionization always develops in high electrical field. This results in high concentration of plasma behind the front. (A simple evaluation in the spirit of Ref. 22 gives $N_d(v_f/v_s)$ as a lower bound for plasma concentration.) In contrast, for uniform breakdown an increase of concentration is immediately followed by a decrease of electrical field due to the coupling to the external load, and high concentrations never can be reached. Therefore the collision between the two fronts should be avoided in applications.

After the switching the voltage at the device exhibits small amplitude oscillations (see Fig. 2). These oscillations are due to a sequence of impact ionization breakdowns near the right boundary of the $n-$base, in the vicinity of the $p^+ - n-$junction. The mechanism of these breakdowns is as follows. As we mentioned in Sec. IIIC,

the voltage at the reversely biased $p^+ - n-$junction starts to recover already during the stage of front propagation. This happens due to the separation of electrons and holes near the $p^+ - n-$junction. Whereas electrons leave this area drifting to the left, holes that drift to the right are constantly supplied by the plasma region. This leads to the formation of a positively charged region at the right side of the $n-$base. Due to the high concentration of holes $p \gg N_d$, the slope of the electrical field $dE/dz = q(p + N_d)/\varepsilon\varepsilon_0$ in this region is orders of magnitude higher than in the depleted region. Thus the threshold of impact ionization E_a at the right boundary can be reached again. As soon as it happens, an electron package, or an avalanche, is generated at the right boundary and the field again drops below the threshold. Due to the generated current pulse the voltage at the device decreases. The electrical field remains below the threshold during the drift of the electron package to the left. Then the field increases again and the next avalanche is generated. (This mechanism resembles the mechanism of IMPATT (for "Impact Ionization Avalanche Transit Time") oscillations known in microwave electronics[18,19]). This process is not sufficient for supporting the conduction state of the device and small amplitude oscillations are accompanied by a gradual increase of the average voltage.

E. Applicability of the continuum appoximation

Above we have shown that in unbiased structures the front is triggered by holes which are generated in the neutral layer and then drift through the depleted layer to the p^+- contact where the electrical field takes its maximum value. When modelling the triggering process in the continuum approximation, we face a crucial problem related to so small hole concentrations that the continuum approximation ceases to be valid. This problem manifests itself in the following *artefact*: impact ionization by electrons in the neutral layer generates holes with the unphysically small concentration $p \ll V^{-1}$, where V is the system volume. These fraction of holes drift towards the p^+-contact where their concentration grows exponentially in the high electrical field, reaches the physically relevant level $p \gg V^{-1}$ and eventually triggers the propagation of the impact ionization front. Consequently, the simulations predict that the front is triggered by any concentration of free carriers generated in the neutral area, even if this concentration corresponds to a small fraction of a hole in the complete volume of the device. This result might be either quantitatively or qualitatively wrong: in the first case the front is predicted to start too early and therefore it propagates at a lower voltage. In the second case, impact ionization in the neutral area is in fact totally incapable of triggering the front because the electrical field is unsufficient. Thus straightforward modeling in the framework of the continuum approximation might

lead to qualitatively wrong results. Since the velocity of the superfast front depends only logarithmically on the background ionization level in the depleted region[22], such simulations give plausible results for the front velocity and the switching time, and the mistake is hard to detect.

In order to overcome this problem, we propose the modified generation term (10) which incorporates the cut-off of the ionization reaction for unphysically low concentrations. The threshold concentrations n_{cut}, p_{cut} are related to the lowest relevant concentrations which can be treated in continuum approximation. To check the relevance of such an approach, we have studied how the solutions depend on n_{cut}, p_{cut}. The example described in the previous section has been calculated for $n_{cut} = p_{cut} = 10^9 \, \text{cm}^{-3}$ which corresponds to an average distance between carriers $\sim 10 \, \mu$m. In Fig. 4 this transient is shown again in curve 3, whiles curves 1, 2 and 4 show the same process, but with $n_{cut} = p_{cut} = 0, 10^6, 10^{10} \, \text{cm}^{-3}$, respectively. Regardless to the cut-off level, the superfast switching remains qualitatively the same and the main phases of the process are the same. Quantitatively, however, for lower cut-off the switching process starts earlier, develops more slowly and results in a higher residual voltage. All these effects are due to the earlier start of the impact ionization front that, in turn, leads to a slower propagation in a lower electrical field and a well-developed collision of ionization and extraction fronts. We conclude that though the continuum model is not capable to provide accurate quantitative predictions, our results are essentially robust with respect to the cut-off level. In the case under consideration, the impact ionization in the neutral area is indeed sufficient for triggering the front.

In Fig. 5 we show the amount of holes generated in the neutral region as a function of the voltage ramp A for different regimes. The hole concentration vanishes with decreasing A, especially in initially biased structures (Fig. 5 (b,c)), and the corresponding triggering mechanism ceases to exist. One of the important implications of the Fig. 5 is that the minimal physical model evaluated in this article is not capable to describe switching of impact ionization fronts for the conditions of the original experiments[23-25]: long ($W > 200 \, \mu$m) and initially biased structures ($V_0 > 400 \, V$) and moderate voltage ramps $A \sim 1 - 2 \, \text{kV/ns}$. Sec. VI contains a further discussion of this problem.

IV. DEPENDENCE ON THE STRUCTURE AND CIRCUIT PARAMETERS

A. Influence of the system length

In Fig. 6(a), the transient $U(t)$ is shown for different system lengths $W = 50, 100, 150, 200$ and $250 \, \mu$m (curves 1, 2, 3, 4 and 5, respectively). All other pa-

rameters are kept as in the basic example in Sec. III. With decrease of the system size the switching occurs earlier and develops faster. In shorter structures, the initial nucleus of electron-hole plasma becomes large compared to the system size W and a substantial voltage drop takes place already at the nucleation phase, whereas the stage of front propagation becomes less pronounced. As a result the fine stucture of the $U(t)-$transient disappears, and the voltage at the device during the switching drops smoothly. Since the extraction front reaches the n^+-contact earlier, the ionization front and the extraction front do not collide. Rather the ionization front propagates over the whole length of the $n-$base. This fact together with the higher average electrical field in a short structure, efficiently create a high conductivity throughout the whole structure and make the residual voltage as low as 70 V for $W = 50$ μm (Fig.6(a), curve 1).

In long structures the collision of ionization front and extraction front is unavoidable. Since the growth of conductivity by quasiuniform ionization after this collision is less efficient than the previous process, the residual voltage increases and becomes as large as 800 V for $W = 250$ μm (Fig. 6(a), curve 5). Next, in presence of a thick neutral layer which acts as an internal Ohmic resistance, the voltage on the device at the initial stage of front propagation even increases. As a result, the inflection of the $U(t)-$dependence (curve 3) that corresponds to the transition from the nucleation stage to the front propagation stage, grows further (curve 4), and the dependence can even become non-monotonic (curve 5).

The maximum voltage at the device increases almost linearly from 1.3 kV to 4 kV with the system length. The voltage ramp during the switching $|(dU/dt)_{down}|$ has its maximum value of $10\,\text{kV/ns}$ for $W = 100, 150$ μm. It decreases with both increase and decrease of the system length to values of $8.9\,\text{kV/ns}$ and $7.4\,\text{kV/ns}$ for $W = 50\,\mu$m and $W = 250\,\mu$m, respectively. In summary, shorter structures switch faster and have a lower residual voltage but commutate less power per pulse.

B. Influence of the voltage ramp

In Fig. 6(b) we present $U(t)-$transients for different voltage ramps while all other parameters are kept as in the basic example. The maximum voltage at the device at the moment of switching is about ~ 2.8 kV for all transients, whereas the delay time, the switching time and the residual voltage are substantially different.

An increase of A leads to a higher electrical field and a more efficient generation of initial carriers in the neutral layer. The ionization front is triggered earlier. Then unavoidably ionization front and extraction front collide. As a result, the residual voltage increases and reaches ~ 800 V for $A = 4$ kV/ns (Fig. 6(b), curve 4).

A decrease of the voltage ramp A increases the delay of switching and ensures that the ionization front passes through the whole length of the $n-$base, so that the residual voltage is low (~ 200 V for $A = 1.6$ kV/ns). However, with a further decrease of A we do not observe triggering anymore since the electrical field in the neutral region region becomes too low to generate initial carriers.

In the next section we discuss the mechanism of superfast front propagation and relate the ionization fronts in layered structures to other ionization fronts and streamers in gases and solids.

V. TRIGGERING AND PROPAGATION OF THE SUPERFAST FRONT

A. The mechanism of propagation

The mechanism of superfast ($v_f > v_s$) propagation of the ionization front is based on generation of electron-hole plasma by the impact ionization followed by screening of the applied electrical field due to the Maxwell relaxation. Due to the propagation of the front, the temporal sequence of plasma generation and screening becomes a spatial sequence. Fig. 7 shows the inner structure of the propagating front: the electric field profile, the concentration profiles, the generation term G (10) and the space charge of the mobile carriers are shown at some instant of time. On the left, the electrical field increases due to the space charge of naked donors, while the space charge of mobile carriers is negligible. The impact ionization wave consists of an impact ionization region ($G > 0$, see curve 5) followed by a region of electric screening (see curve 4). The position of the screening region roughly coincides with the concentration front - the edge of the plasma region. The density of mobile carriers in the impact ionization region increases until the electric field is screened by the Maxwell relaxation of the generated electron-hole plasma. Due to the *pre-ionization* (a small amount of mobile carriers in the depleted layer), the edge of the plasma region can move faster than the drift velocity of the individual carriers due to the local multiplication of existing carriers. In the system under consideration, these initial carriers are holes that are being generated by impact ionization in the neutral layer on the left and that drift into the high-field region on the right. (Alternative sources of initial carriers that can become important for other experimental situations are discussed in Sec. VI.) In the screening region, the presence of excessive negative charge is clearly visible since the concentration of electrons is higher then the concentration of holes (see also Fig. 3(c)).

The mechanism of propagation is essentially the same for finger-shaped streamers in pre-ionized gases and solids[6,7,10−12] and plane fronts in p^+-n-n^+-structures. Recently superfast streamer fronts have also been found in numerical investigations of Corbino disks made from GaAs films[44,45]. If the pre-ionization is rather homogeneous, a propagating front with finite length can emerge

due to the spatial profile of the electric field: the electrical field, which exceeds the threshold of impact ionization near the front, should be below the threshold at a certain distance from the front. This provides a finite size of the "active zone", where the impact ionization develops, and prevents uniform blow-up of the concentration in the whole sample[46]. For finger-like streamers, such a field profile is due to the Coulomb decrease of the electrical field with increasing distance from the space charge located at the streamer tip [11,12]. For radially symmetrical fronts in Corbino disks, the decrease of the electrical field $E \sim r^{-1}$ results from the geometry of the concentrical two-dimensional sample[3]. In the case under consideration, the electrical field decreases linearly like $dE/dz = qN_d/\varepsilon\varepsilon_0$ due to the space charge of the naked donors in the depleted layer. The superfast ionization front in the $p^+ - n - n^+-$structure should be regarded as a plane streamer-like front propagating into a charged low-conducting layer.

B. The avalanche-to-streamer transition

The excitation of the superfast impact ionization front in a semiconductor structure corresponds to the transition from the conventional *avalanche* scenario of impact ionization breakdown[18,19], where electrons and holes drift apart in the applied electrical field, to a new scenario, where the collective dynamics of electron and holes results in screening of the applied field in some region. It is known from experiments[23,24,26] and has been confirmed by our numerical simulations that this *avalanche-to-streamer* transition takes place only if the voltage applied to the semiconductor structure increases faster than a certain threshold value $A_{th} \sim 10^{12}$ V/s. A threshold for the voltage ramp also exists for finger-like streamers in sufficiently pre-ionized gases and in solids[7,11,12]. In the case of a streamer in a bulk semiconductor that is triggered from a needle electrode[7], the threshold value has the same order of magnitude of 10^{12} V/s. Thus a sufficient voltage ramp represents a general condition for an avalanche-to-streamer transition in a pre-ionized medium[47].

The existence of the critical voltage ramp can be understood qualitatively if we assume that the pre-ionization is uniform over the whole sample, and thus that the carrier multiplication starts as soon as the electrical field near the electrode reaches the threshold value E_a [11]. During the triggering stage, when the electron-hole plasma has not been created yet and the space charge of mobile carriers remains negligible, the "active zone", where the field exceeds the effective threshold of impact ionization and carriers are generated, expands with increasing applied voltage. If the edge of the active zone moves faster than the drift velocity, the generated carriers remain in the "active zone" and all of them, first, further contribute to impact ionization and, second, contribute to screen-

ing. Due to this trapping of the mobile carriers in the "active zone", the initial nucleus of electron-hole plasma can be formed. If the condition is not met, carriers drift apart in the applied electrical field, forming a common avalanche, and the avalanche-to-streamer transition does not occur. The fast expansion of the active zone requires the application of a sufficiently sharp voltage ramp.

It has been shown recently[48] that for the $p^+ - n - n^+-$structure the order of magnitude value of the critical voltage ramp is given by

$$A_{th} \approx E_a v_s. \tag{13}$$

Eq.(13) bears a strong similarity to the approximate condition obtained for finger-like streamers propagating from tip metal contact in bulk semiconductor obtained in Ref. 11:

$$A \approx \frac{E_0\, v_s}{ln(\alpha_0 R)}, \tag{14}$$

where it is assumed that impact ionization coefficients are given by the expression $\alpha(E) = \alpha_0\, exp(-E_0/E)$ for both electrons and holes, and R is the radius of the metal tip used as a contact.

VI. DISCUSSION

A. The source of initial carriers

If the voltage ramp A applied to an initially unbiased structure is sufficiently large, impact ionization in the neutral region is the dominant source of initial carriers. The high density $n \approx N_d$ of electrons in the neutral region generates even in low fields a relatively high concentration of holes that will trigger the front after traveling through the $n-$base. Hence triggering here can be considered as a deterministic process. Its time delay is determined by the generation time of holes in the neutral region and their travel time through the $n-$base. Our model here appropriately captures the physical mechanisms.

The behavior changes drastically when the applied voltage ramp A is decreased and the initial bias V_0 is increased. The electrical field in the neutral region then becomes too low to generate a sufficient amount of holes and the front triggering fails. In Fig. 5 we show the maximum concentration of holes generated in the neutral region. This figure allows to identify in which parameter regimes front triggering due to this mechanism is possible.

It is remarkable, that this triggering mechanism turns out to be ineffective for the parameters corresponding to the original experiments[23-25]: high initial bias $V_0 \sim 600...1000$ V, long $n-$base length $W \sim 220...250\,\mu$m and moderate voltage ramps $A \sim 1$ kV/ns. This result is in agreement with analytical estimates[49] but in contradiction with earlier numerical simulations[50,51,28] which

have been performed in the framework of the same drift-diffusion model (1), (2), (3), but without cut-offs for low concentrations in (10). The analysis of the triggering stage shows that the switching observed in Ref. 50, 51 is unphysical and due to the multiplication of too small concentrations of mobile carriers, that either appear due to impact ionization in the neutral region or are assumed to be present in the depleted layer due to the thermal generation. These concentrations correspond to fractions of electrons and holes and can not be captured in a continuum approximation, as discussed in Sec. IV.E. The numerical solutions from Ref. 50, 51 can not be reproduced for any meaningful cut-off n_{cut}, p_{cut} in the generation term (10). In particular, for parameters in Ref. 50 — $W = 200\,\mu\mathrm{m}$, $A \sim 1 - 2\,\mathrm{kV/ns}$ — triggering of the front can not be explained. For parameters chosen in Ref. 51 — $W = 220\,\mu\mathrm{m}$, $A > 3\,\mathrm{kV/ns}$ — impact ionization in the neutral area is in principle sufficient to trigger the front, but numerical simulations with cut-offs show that the initial nucleus of electron-hole plasma is created not near the p^+-contact, but in the middle of the depleted layer. The triggering occurs after a much longer delay (~ 2 ns) than the one reported in Ref. 51 (less than 1 ns). This nucleus then expands towards the n^+-contact, in the direction where the pre-ionization is present, as a superfast front, and towards the p^+-contact, where there is no pre-ionization, as a slow front which moves with the drift velocity. Due to the low velocity of the second front this process does not lead to the experimentally observed superfast switching[23,49,25]. Ref. 28 uses the same drift-diffusion model as Ref. 50, 51, but it lacks information about the set of parameters used in the simulations, and thus does not allow a comparison with our simulations.

This discrepancy with the experiments[23–25] with initial bias indicates that another source of initial carriers becomes important. The first source to be discussed — and excluded — is thermal generation in the depleted layer. This estimate is based on the value $J \sim 10^{-7}\,\mathrm{A/cm^2}$ of the thermally generated current density at room temperature in a reversely biased structure [23]. It corresponds to a concentration of thermal carriers of $n, p \sim 10^6\,\mathrm{cm^{-3}}$. This concentration is below a continuum approximation: the average distance between carriers exceeds $100\,\mu\mathrm{m}$ and the average interval between two generation processes is longer than 1 ns. These spatial and temporal scales coincide with the longitudinal size of the system and the time scale of the whole switching process, respectively. Thus the avalanche process triggered by thermal carriers, first, would be stochastic, and, second, would result in local switching but not in switching of the whole cross-section of the device. In contrast, the experiments[23–25,27] show neglible deviation from one switching to another (small jitter) and indicate that a sufficiently homogeneous switching over the whole cross-section of the device can be achieved[52].

An alternative source of initial carriers can be suggested if we take into account that the Si diode structures studied experimentally in Refs. 23–25, 27 were manufactured according to the standard technology generally used for fabrication of power semiconductor devices. Later on this technology has been shown to have a side effect [53,54]: it creates a specific type of process-induced deep level defects. These defects appear in the $n-$base during the heat treatment of the sample while a deep $p - n-$junction is formed[53,54]. It has been suggested that these deep levels correspond to the double donor levels of isolated sulfur centers[53,54]. The respective midgap level, coined as M-center[53–56], has a ionization energy $E_M = 0.54$ eV (the band gap width in Si $E_g = 1.12$ eV)[53]. The concentration of M-centers even in high purity n-doped samples lies in the interval $10^{11} - 10^{13}$ cm^{-3}, thus comparable to the donor concentration $N_d \approx 10^{14}$ cm^{-3}, and their distribution over the sample is reasonably uniform[53]. The most important feature of the M-center is a strong asymmetry between the electron and hole capture cross-sections: $\sigma_n = 10^{-15}$ cm^{-3} and $\sigma_p = 10^{-20}$ cm^{-3}, respectively[53]. This asymmetry has two consequences: First, it makes the M-center a perfect *electron trap*, since only the electron transiton from the M-center to the conductance band and back is allowed. Second, due to the low cross-section of hole capture, M-centers do not assist the recombination and hence do not influence the life time of the nonequilbrium carriers - one of the most important characteristic of the material in the device applications. Therefore their presence in the sample is generally not controlled in fabrication, and is even widely unknown. Capacitance transient spectroscopy studies[53] have also revealed two other types of process induced deep-level defects with ionization enegies 0.28 eV and 0.34 eV, coined as U- and L-centers, respectively. Like M-centers, U- and L- centers are also electron traps with low recombination acitivity, though the asymety of the cross-sections of electron and hole captures is much less pronounced.

We propose that M-centers represent the most probable source of initial carriers for triggering the impact ionization front in initially biased structures for low voltage ramps. The respective level lies below the Fermi level in an n-doped sample and hence M-centers are occupied at room temperature and in low electrical fields. When a strong electrical field is applied, trapped electrons are released to the conductance band by a tunneling process. The threshold of tunneling ionization of a midgap deep center is expected to be above the threshold of band-to-band impact ionization ($\sim 2 \cdot 10^5$ V/cm in Si) but well below the threshold of band-to-band tunneling ionization ($\sim 10^6$ V/cm in Si). Tunneling ionization of M-centers starts near the p^+-contact, where the electrical field takes its maximum value, and then develops throughout the $n-$base, thus providing initial carriers both for triggering and for the superfast propagation of the impact ionization front. It is possible that the tunneling ionization of U- and L-centers is also essential. The corresponding model is presently under investigation.

B. Optimal performance in pulse sharpening applications

Triggering of superfast impact ionization fronts in Si diodes has found important applications in pulse power electronics for sharpening of electrical pulses[26−28]. The most important characteristics of these sharpening devices are the ratio between the rate of voltage drop at the device during switching and the initially applied voltage ramp A — the so-called sharpening coefficient —, the switching time, the power per pulse and the residual voltage. Our one-dimensional simulations show that one of the key points for the optimal performance is to avoid the collision between the impact ionization and extraction fronts. Such a collision inevitably leads to higher residual voltages and longer switching times. The $n-$base length W and the applied voltage ramp A should be chosen appropriately. The collision generally takes place in long structures when the extraction front needs a long time to travel through the $n-$base. However, a decrease of W lowers the maximum voltage at the device and, hence, the power per pulse. For high voltage ramps A, the collision of impact ionization and extraction fronts is due to an earlier triggering of the ionization front because of the higher rate of impact ionization in the neutral area. Neither the switching time nor the maximum voltage show a strong dependence on A, so the best sharpening coefficient can be achieved for the lowest value of A that still allows for a deterministic triggering of the front. The initial voltage V_0 also can be used as a tuning parameter. With increasing V_0, the initial position of the extraction front shifts towards the n^+-contact. Our simulations show that in certain regimes even the small initial bias $V_0 = 50...100$ V can be sufficient to avoid the collision and to substantially improve the switching characteristics.

However, another effect of the extraction front comes into consideration when transverse degrees of freedom are taken into account. In large-area structures, whose transverse dimension (diameter) d exceeds the $n-$base length W, a transverse instability of ionization front should be expected [35−37]. This instability eventually leads to current localization and formation of local switching channels, as has been observed experimentally in Ref. 34. It has been predicted[37] that ionization fronts propagating into a fully depleted $n-$base are strongly unstable, wheras in in presence of the extraction front this transverse instability is suppressed. Therefore in large-area structures the extraction front might have a two-fold effect: on the one hand, the collision of ionization and extraction fronts is to be avoided, on the another hand, the presence of the extraction front is important for transverse stability. We propose that the optimal performance can be achieved when the ionization front and extraction front reach the n^+-contact simultaneosly, and thus both conditions above are satisfied.

C. Ionization fronts in bulk semiconductors

Our numerical simulations show that superfast impact ionization fronts, that traditionally have been triggered in initially biased $p^+ - n - n^+-$structures, in fact can be triggered succesfully by applying the voltage ramp to an equilibrium structure without initial bias. This finding indicates a new possibility to trigger similar superfast fronts in *bulk samples* without any $p - n-$junction. Indeed, originally layered $p^+ - n - n^+-$structures have been used mainly, because the $p^+ - n-$junction can support the initial voltage V_0. This ceases to be necessary when the device is operated without initial bias. Since all relevant processes develop inside the uniformly doped $n-$base, triggering and propagation of impact ionization front might be achieved in a bulk $n-$doped sample, as long as the contacts allow the extraction of electrons from the sample during the delay stage.

VII. SUMMARY AND CONCLUSIONS

When a sharp voltage ramp is applied to an initially unbiased $p^+ - n - n^+-$structure switched in series with a load resistance R, after some delay an impact ionization front is triggered. It propagates from the p^+-contact to the n^+-contact, leaves a dense electron-hole plasma behind and thus switches the diode structure into a high conductivity state. During the delay period the major carriers (electrons) are being extracted from the $n-$base. This happens through the propagation of an extraction front which moves towards the n^+-contact with the electron drift velocity. The extraction front separates the expanding depleted layer near the p^+-contact from the shrinking neutral layer near the n^+-contact where the major carriers still are present. The electrical field in the structure increases and overcomes the effective threshould of impact ionization near the p^+-contact, but an avalanche breakdown in the depleted layer can not develop due to the absence of initial carriers. Rather a considerable impact ionization reaction starts in the neutral layer where the electron density is high. The generated holes drift from the neutral region through the depleted layer towards the p^+-contact. Avalanche impact ionization by these holes then starts as soon as the holes reach the region of high electrical field near the p^+-contact. Provided that the applied voltage ramp exceeds the threshold value $A \sim E_a v_s \sim 10^{12}$ V/s, we observe the onset of the streamer mode of impact ionization breakdown instead of the usual mode of avalanche breakdown. The streamer mode is characterized by an efficient screening of the applied electrical field from the generated electron-hole plasma. Already the formation of the initial nucleus of electron-hole plasma near the p^+- contact is accompanied by a substantial drop of the voltage on the device. This drop is due to the interaction with the external load as the current increases. The

voltage on the device continues to decrease as the initial nucleus expands towards the n^+-contact by means of an impact ionization front. The front propagation is a collective process, based on the generation of free carriers by impact ionization and on Maxwell relaxation in the plasma behind the front. Thus the drift velocity of individual carriers does not limit the front velocity which can become several times faster than the saturated drift velocity v_s. The presence of initial carriers in the depleted region of the ionization front is a necessary condition for the superfast propagation with $v_f > v_s$. This background ionization is created by impact ionization in the neutral layer. Since the velocity of the impact ionization front exceeds the velocity of the extraction front, collision between these two fronts is possible. This collision implies that the ionization front reaches the neutral area with high concentration of major carriers (electrons). This terminates the front propagation, and the remaining part of the structure undergoes a quasi-uniform breakdown.

The impact ionization breakdown in an initially unbiased structure has been demonstrated to develop qualitatively in the same way as it has been believed to develop in heavily biased structures[23,24,26,28]. The reason of this similarity is the delay in the front triggering, which takes place due to the absence of initial carriers in the high field area and provides time for the extraction front to travel along the $n-$base and to form the depleted layer. As a result, at the moment when the ionization front is triggered, the field and the concentration profiles in the device are similar to those in the initially biased structures. The essential difference between these two regimes is the triggering mechanism. For initially unbiased structures, during the delay stage the electrical field in the neutral area reaches substantially higher values. Thus the impact ionization by major carriers (electrons) in the neutral area is very efficient and capable to provide a sufficient supply of initial carriers to trigger the front. In contrast, in initially biased structures this mechanism is unefficient. We propose that tunneling ionization of deep electrons traps (M-centers, see Ref. 53, 54), which are present in the Si structures studied in experiments[23,24], is responsible for triggering the front in initially biased structures.

We have shown that the limits of continuum approximation should be properly taken into account when modeling the process, since the multiplication of unphysically small concentrations by impact ionization easily leads to qualitatively wrong results. The inherent presence of small densities of free carriers together with their important role during the earlier stages of the process makes the continuous drift-diffusion model insufficient for accurate quantitative description of the process. We have shown that in certain cases these problems can be overcome by introducing cut-offs for small concentrations in the generation term.

The superfast ionization fronts in layered semiconductor structures belong to the large family of streamer fronts like finger-shaped streamers and plane streamer-like fronts in gases and solids and have the same mechanism of propagation as any streamer front propagating into pre-ionized media. The essential difference is that in a layered doped structure the front propagates not into a neutral but into a spatially charged depleted layer.

[1] *Dynamics of Curved Fronts,* edited by P. Pelce (Academic Press, Boston, 1988).

[2] M. S. Cross and P. C. Hohenberg, Reviews of Modern Physics, **65**, 853 (1993).

[3] E. Schöll, *Nonlinear Spatio-temporal Dynamics and Chaos in Semiconductors* (Cambridge University Press, Cambridge, 2000).

[4] H. Raether, Z. Phys. **112**, 464 (1939) (in German); H. Raether, *Electron avalanches and breakdown in gases*, (Butterworths, London, 1964).

[5] *Electrical Breakdown in Gases*, edited by J.M. Meek and J.D. Craggs (Wiley, 1978).

[6] L. B. Loeb, Science **148**, 1417 (1965).

[7] N. G. Basov, A. G. Molchanov, A. S. Nasibov, A. Z. Obidin, A. N. Pechenov, and Yu. M. Popov, Sov. Phys. JETP, **43**, 912 (1976) [Zh. Eksp. Teor. Fiz. **70**, 1751 (1976)].

[8] E. M. Bazelyan, Yu. P. Raizer, *Spark Discharges* (CRS Press, New York, 1998).

[9] Yu. P. Raizer, *Gas Discharge Physics* (Springer, Berlin, 1997).

[10] S. K. Dhali and P. F. Williams, Journal of Applied Physics **62**, 4696 (1987).

[11] M. I. D'yakonov and V. Yu. Kachorovskii, Sov. Phys. JETP **67**, 1049 (1988). [Zh. Eksp. Teor. Fiz. **94**, 321 (1988)].

[12] M. I. D'yakonov and V. Yu. Kachorovskii, Sov. Phys. JETP **68**, 1070 (1989) [Zh. Eksp. Teor. Fiz. **95**, 1850 (1989)].

[13] P. A. Vitello, B. M. Penetrante and J. N. Bardsley, Phys. Rev. E **49**, 5574 (1994).

[14] U. Ebert, W. van Saarloos and C. Caroli, Phys. Rev. Lett. **77**, 4178 (1996).

[15] U. Ebert, W. van Saarloos and C. Caroli, Phys. Rev. E. **55**, 1530 (1997).

[16] U. Ebert and M. Arrayás, *Pattern formation in electric discharges*, in: *Coherent Structures in Complex Systems*, edited by D. Reguera, Lecture Notes in Physics (Springer, June 2001). (Preprint: CWI Report MAS-R0028, CWI, Amsterdam).

[17] *Electrical discharges for environmental purposes: fundamentals and applications*, edited by E.M. van Veldhuizen (NOVA Science Publishers, New York, 1999).

[18] S. M. Sze, *Physics of Semiconductor Devices*, (Willey, New York, 1981).

[19] M. Shur, *Physics of Semiconductor Devices*, (Prentice-Hall, Englewood Clifs, 1990).

[20] M. Shaw, V. Mitin, E. Schöll and H. Grubin, *The Physics on Instabilities in Solid State Electron Devices*, Plenum Press, New York, 1992.

[21] H. J. Prager, K. K. N. Chang and J. Wiesbord, Proc. IEEE **55**, 586 (1968).

[22] B. C. Deloach and D. L. Scharfetter, IEEE Transactions Electron Devices **ED-20**, 9 (1970).

[23] I. V. Grekhov and A. F. Kardo-Sysoev, Sov. Tech. Phys. Lett. **5**, 395 (1979) [Pis'ma Zh. Tekn. Fiz. **5**, 950 (1979)].

[24] I. V. Grekhov, A. F. Kardo-Sysoev, L. S. Kostina and S. V. Schenderei, Electron. Lett. **17**, 422, (1981); Sov. Techn. Phys. **26**, 984 (1981) [Zh. Techn. Fiz. **51**, 1709 (1981)].

[25] D. Benzel, M. Pocha, Rev. Sci. Inst. **56** 1456 (1985).

[26] I. V. Grekhov, Sol. St. Electron. **32** , 923 (1989).

[27] A. F. Kardo-Susoev, V. M. Efanov and I. G. Chashnikov, *Fast power switches from picosecond to nanosecond time scale and their application to pulsed power* in *Dig. Techn. Papers, 10th IEEE Int. Pulsed Power Conf.*, edited by W. L. Baker and G. Cooperstain, Albuquerque, 1995, pp.342-347.

[28] R. J. Focia, E. Schamiloglu, C. B. Fledermann, F. J. Agee, J. Gaudet, IEEE Transaction on Plasma Science, **25**, 138 (1997).

[29] I. V. Grekhov, V. M. Efanov, A. F. Kardo-Susoev, I. A. Smirnova, Sov. Tech. Phys. Lett. **11**, 372 (1985) [Pis'ma Zh. Techn. Fiz. **11**, 901 (1985)].

[30] V. A. Kozlov, A. F. Kardo-Susoev and V. I. Brulevsky, Semiconductors **35**, 608 (2001) [Fiz. i Techn. Poluprov. **35**, 629 (2001)].

[31] Zh. I. Alferov, I. V. Grekhov, V. M. Efanov, A. F. Kardo-Susoev, V. I. Korol'kov, M. N. Stepanova, Sov. Tech. Phys. Lett. **13**, 454 (1985) [Pis'ma Zh. Techn. Fiz. **13**, 1089 (1987)].

[32] I. V. Grekhov and V. M. Efanov, Sov. Tech. Phys. Lett. **14**, 920 (1988) [Pis'ma Zh. Techn. Fiz. **14**, 2121 (1988)].

[33] I. V. Grekhov and V. M. Efanov, Sov. Tech. Phys. Lett. **16**, 645 (1990) [Pis'ma Zh. Techn. Fiz. **16**, 9 (1990)].

[34] S. N. Vainstein, Zu. V. Zhilyaev, M. E. Levinstein, Sov. Tech. Phys. Lett. **14**, 664 (1988).

[35] A. Minarsky and P. Rodin, Techn. Phys. Lett. **20**, 490 (1994) [Pis'ma Zh. Tekh. Fiz. **20**, 38 (1994)].

[36] A. Minarsky and P. Rodin, Sol. St. Electron., **41**, 813 (1997).

[37] A. Minarsky and P. Rodin, Semiconductors **31**, 366-370 (1997) [Fiz. Tekh. Poluprovodn. **31**, 432 (1997)].

[38] H. Jalali, R. Joshi, J.A. Gaudet, IEEE Transactions on Electron Devices, **45**, 1761 (1998).

[39] A. Wacker and E. Schöll, J. Appl. Phys. **78**, 7352 (1995).

[40] C. Jacobini, C. Canali, G. Ottaviani and A. Alberigi, Sol. Stat. Electron. **20**, 77 (1977).

[41] V. A. Kuz'min, N. N. Krukova, A. S. Kuregyan, T. T. Mnatsakanov and V. B. Shuman, Sov. Phys. Semicond. **9**, 481 (1975) [Fiz. Tekh. Poluprovodn. **9**, 735 (1975)].

[42] J. C. Strikwerda, *Finite difference schemes and partial differential equations*, (Chapman & Hall, New York, 1989).

[43] J. G. Verwer, W. Hundsdorfer, J. G. Blom, *Numerical time integration for air pollution models*, Surveys on Mathematics for Industry, Vol. 10/4 (2001). (Preprint: CWI Report MAS-R9825, CWI, Amsterdam.)

[44] G. Schwarz, C. Lehmann, and E. Schöll, Phys. Rev. B **61** 10194 (2000).

[45] G. Schwarz, *Current Filamentation in Doped GaAs Corbino Disks*, Ph.D. Thesis, TU Berlin, 2000. (URL: $http://edocs.tu-berlin.de/diss/2001/schwarz\_georg.pdf$)

[46] Note, that the spatial structure of a propagating front also can be created by a spatially decaying pre-ionization in a constant electric field in a planar geometry[15,16].

[47] As has been discussed in Sect. IV.B, in our specific system the voltage ramp A also controls the generation of initial carriers in the neutral layer. The effect of A we consider here is of different origin, and more generic.

[48] A. Minarsky and P. Rodin, Semiconductors **34**, 665-667 (2000) [Fiz. Tekh. Polupr. **34**, 692 (2000)].

[49] I. V. Grekhov, A. F. Kardo-Sysoev, M. V. Popova and S. V. Shenderei, Soviet Physics – Semiconductors **17**, 877 (1983) [Fiz. Tekh. Poluprovodn. **17**, 1380 (1983)].

[50] Yu. D. Bilenko, M. E. Levinstein, M. V. Popova and V. S. Yuferev, Soviet Physics – Semiconductors **17**, 1156 (1983) [Fiz. Tekn. Poluprovodn. **17**, 1812 (1983)].

[51] A. F. Kardo-Sysoev and M. V. Popova, Semiconductors **30**, 431 (1996) [Fiz. Tekn. Poluprovodn. **30** 803 (1996)].

[52] The inverse frequency of thermal generation in the depleted layer — of the order of 1 ns at room temperature — imposes a limitation on the duration of the latent stage (delay in triggering) that can not exceed several nanoseconds. If the front is not triggered deterministically within this time but the applied voltage continues to increase, thermal carriers will initialize an irregular avalanche breakdown, that is likely to lead to current localization and thermal destruction.

[53] E. V. Astrova, V. B. Voronkov, V. A. Kozlov and A. A. Lebedev, Semicond. Sci. Technol. **13**, 488 (1998).

[54] E. V. Astrova, V. A. Kozlov, A. A. Lebedev and V. B. Voronkov, Solid State Phenomena **69-70**, 539 (1999).

[55] L. D. Yau and C. T. Sah, Solid State Electronics **17**, 193 (1974).

[56] C. T. Sah and C.T. Yang, Journal of Applied Physics **6**, 1767 (1975).
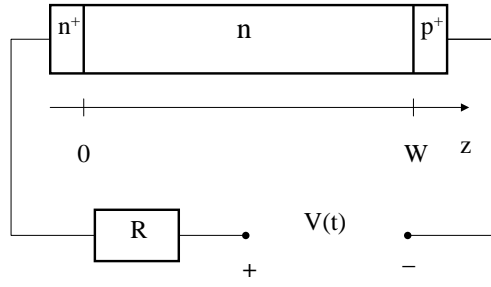
FIG. 1. Sketch of the $p^+ - n - n^+$ −structure operated in an external circuit with load resistance R.
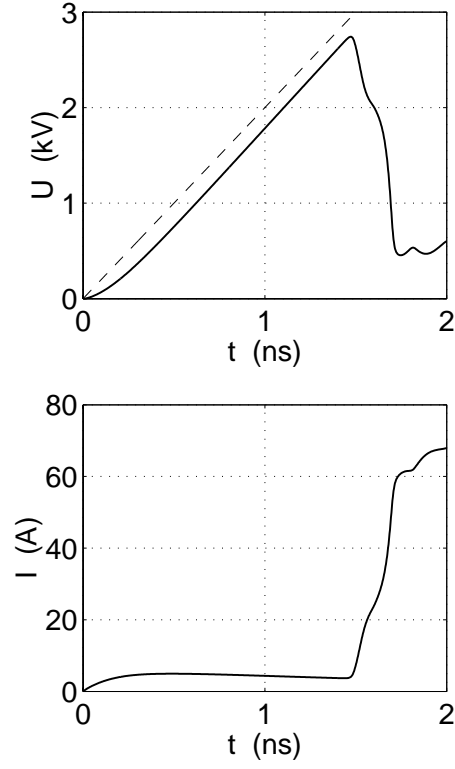
FIG. 2. Voltage at the structure $U(t)$ (solid line in the upper panel) and current $I(t) = S\ J(t)$ (in the lower panel) during the switching process. The dashed line in the upper panel denotes the externally applied voltage $V(t)$. The shown quantities are related through Ohm's law $V = U + RI$. Parameters: $W = 150\ \mu$m, $S = 0.02$ cm^2, $N_d = 10^{14}$ cm^{-3}, $N_a = 0$, $V_0 = 0$, $A = 2.0$ kV/ns, $R = 50\ \Omega$, $n_{cut} = p_{cut} = 10^9$ cm^{-3}.
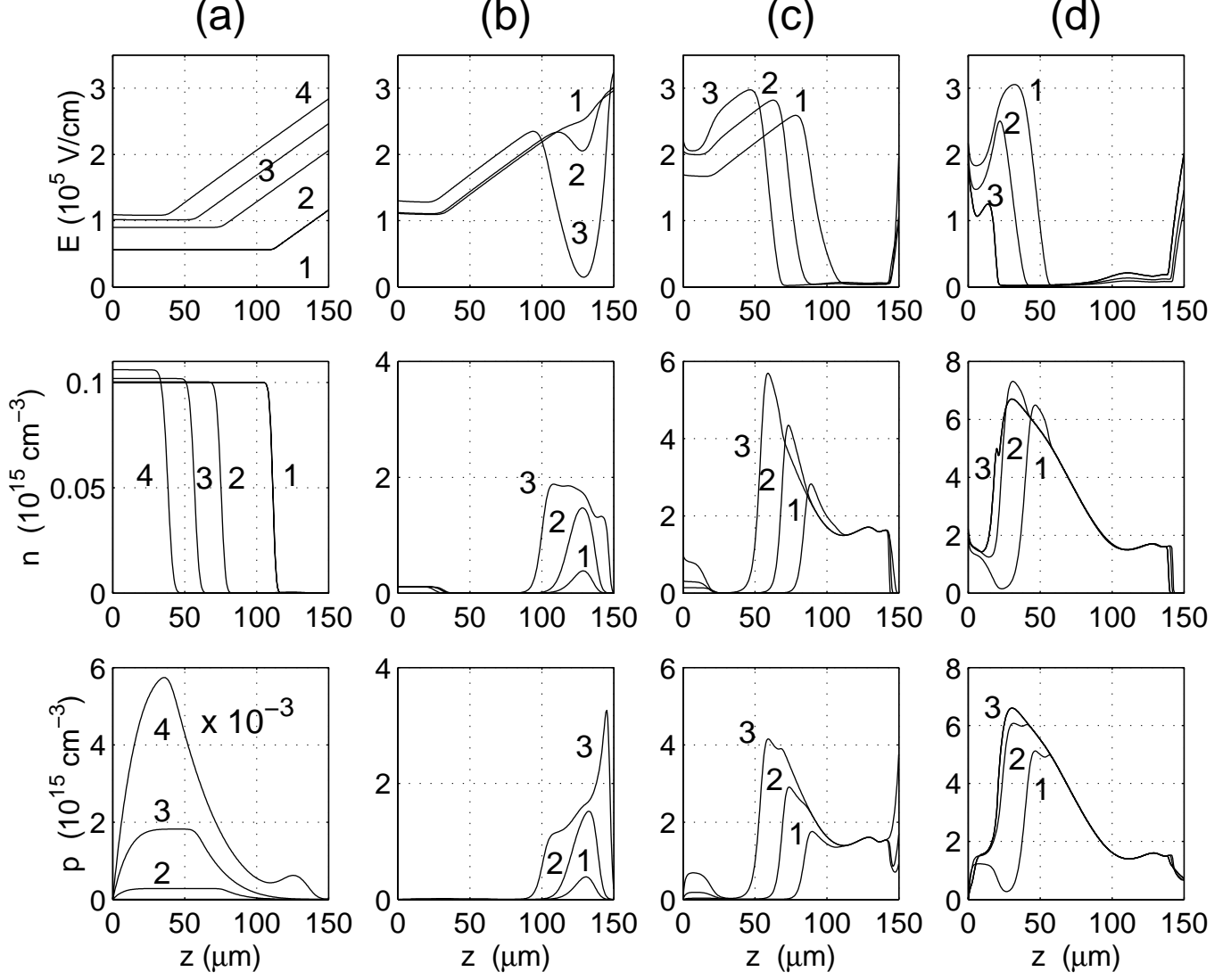
FIG. 3. The internal dynamics leading to the external characteristics of Fig. 2. Shown are the spatial profiles of the electrical field $E(x,t)$ and electron and hole concentrations $n(x,t)$, $p(x,t)$ in the $n-$base ($0 \leq z \leq W = 150\,\mu$m) at different times: (a) propagation of the extraction front and impact ionization in the neutral layer at times $t = 0.6, 1.0, 1.2, 1.4$ ns (curves 1,2,3,4, respectively); (b) nucleation of electron-hole plasma and triggering of the impact ionization front at times $t = 1.47, 1.49, 1.54$ ns (curves 1,2,3); (c) propagation of the impact ionization front at $t = 1.59, 1.63, 1.66$ ns (curves 1,2,3) ; (d) final stage of the switching: collision of impact ionization and extraction fronts, curves 1,2,3 correspond to $t = 1.68, 1.70, 1.73$ ns. All parameters as in Fig. 2. We note that the scale of the hole density p is a factor of 10^{-3} smaller (i.e, 10^{12} cm^{-3}) in column (a) and that we nevertheless skip curve 1 in this paneel, since the the hole density at $t = 0.6$ ns vanishes even on this enlarged scale.
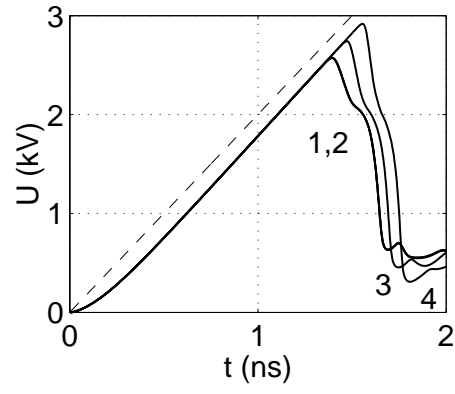
FIG. 4. Voltage at the device $U(t)$ calculated for different cut-offs $n_{cut}, p_{cut} = 0$, 10^6, 10^9, 10^{10} cm^3 (curves 1,2,3,4 respectively.) Curves 1 and 2 coincide within the accuracy of this graph. Other parameters as in Fig. 2.
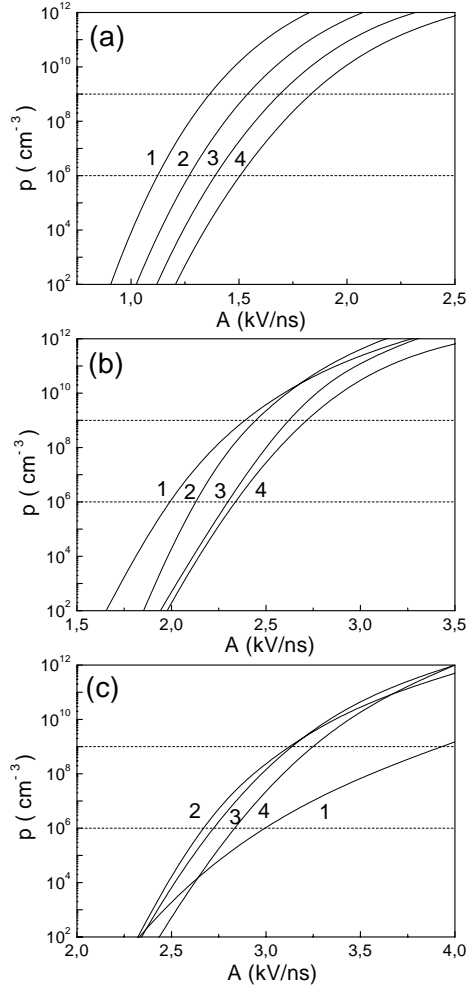
FIG. 5. The maximum concentration of holes generated by impact ionization in the neutral area as a function of the applied voltage A for different initial biases V_0 and system lengths W. Panels (a), (b) and (c) correspond to the initial bias $V_0 = 0$, 400, 1000 V, respectively. Curves 1,2,3,4 correspond to the system lengths $W = 150$, 200, 250, 300 μm, respectively. Below the dashed line at $p = 10^6$ cm^{-3} only few holes or fractions of holes are generated in the system (average distance between carriers $\sim 100\,\mu$m). Above the dashed line at $p = 10^9$ cm^{-3} the concentration of holes is presumably sufficient for deterministic triggering of the impact ionization front (average distance between carriers $\sim 10\,\mu$m).
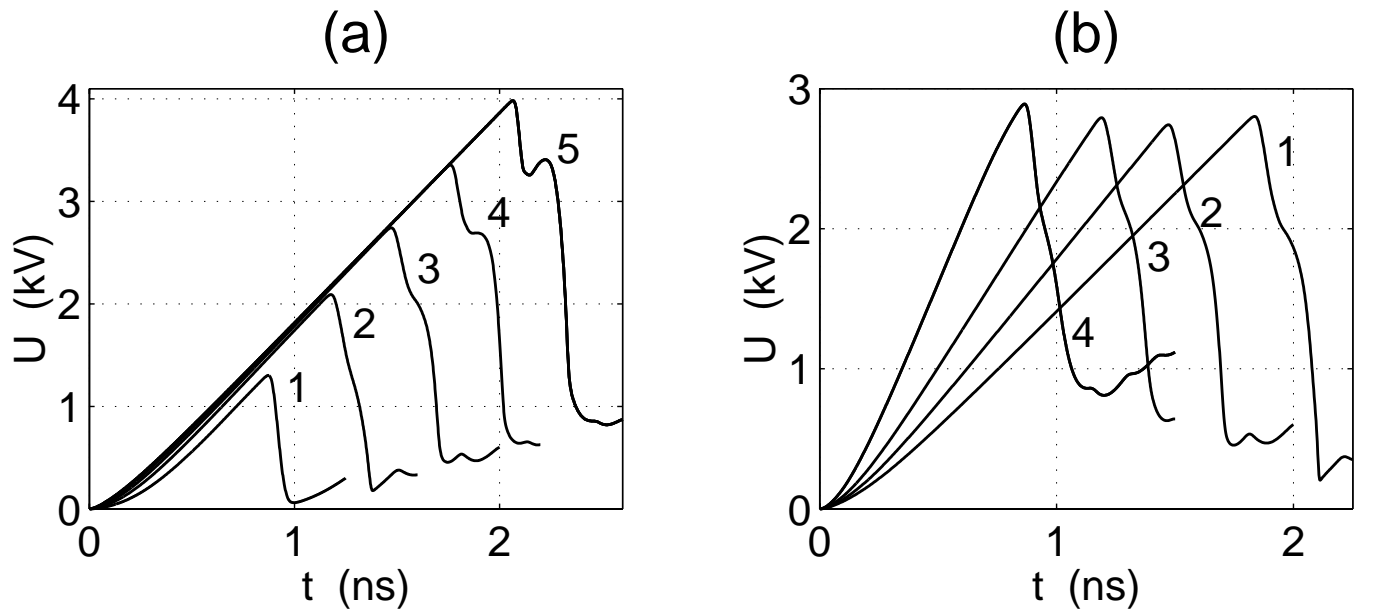
FIG. 6. (a) Voltage at the device $U(t)$ during the switching process calculated for different $n-$base lengths $W = 50, 100, 150, 200, 250\mu$m (curves 1,2,3,4,5, respectively). (b) Voltage at the device $U(t)$ during the switching process for different voltage ramps $A = 1.6, 2.0, 2.6, 4.0$ kV/ns (curves 1,2,3,4). Other parameters as in Fig. 2.
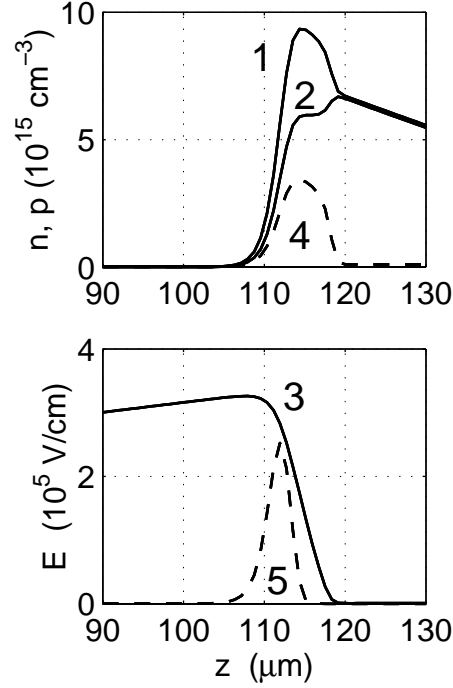

FIG. 7. The inner structure of the superfast impact ionization front. The concentrations of electrons and holes (curves 1 and 2 in the upper panel, respectively) and the electrical field (curve 3 in the lower panel) are shown at the some instant of time. The dashed lines show the difference of electron and hole concentration $(p - n)$ that is proportional to the space charge of mobile carriers (curve 4 in the upper pannel) and the impact ionization rate G (curve 5 in the lower pannel, in arbitrary units).

18